LETTER TO THE EDITOR

Early embryonic lethality in complex I associated *p.L104P Nubpl* mutant mice

Cheng Cheng[1], James Cleak[2], Lan Weiss[1], Heather Cater[2], Michelle Stewart[2], Sara Wells[2], Rod Carlo Columbres[1], Alyaa Shmara[1], C. Alejandra Morato Torres[3], Faria Zafar[3], Birgitt Schüle[3], Jonathan Neumann[4], Eli Hatchwell[5] and Virginia Kimonis[1,6,7,8,9*]

Abstract

Background: Variants in the mitochondrial complex I assembly factor, NUBPL are associated with a rare cause of complex I deficiency mitochondrial disease. Patients affected by complex I deficiency harboring homozygous *NUBPL* variants typically have neurological problems including seizures, intellectual disability, and ataxia associated with cerebellar hypoplasia. Thus far only 19 cases have been reported worldwide, and no treatment is available for this rare disease.

Methods: To investigate the pathogenesis of NUBPL-associated complex I deficiency, and for translational studies, we generated a knock-in mouse harboring a patient-specific variant *Nubpl* c.311T>C; p. L104P reported in three families.

Results: Similar to *Nubpl* global knockout mice, the *Nubpl* p. L104P homozygous mice are lethal at embryonic day E10.5, suggesting that the *Nubpl* p. L104P variant is likely a hypomorph allele. Given the recent link between Parkinson's disease and loss-of-function *NUBPL* variants, we also explored aging-related behaviors and immunocytochemical changes in *Nubpl* hemizygous mice and did not find significant behavioral and pathological changes for alpha-synuclein and oxidative stress markers .

Conclusion: Our data suggest that homozygotes with *Nubpl* variants, similar to the null mice, are lethal, and heterozygotes are phenotypically and neuropathologically normal. We propose that a tissue-specific knockout strategy is required to establish a mouse model of *Nubpl*-associated complex I deficiency disorder for future mechanistic and translational studies.

Keywords: Complex I deficiency, Mitochondria, Parkinson's disease, NUBPL, Mouse model

Introduction

Mitochondrial Complex I deficiency is the third most common mitochondrial disorder in the population. In humans, complex I is composed of 44 different subunits either encoded by nuclear or mitochondrial DNA [1]. More than 16 genes are implicated in mitochondrial complex I assembly [1], and pathogenic variants

in subunits or assembly factors have been implicated in the complex I disorders. Nucleotide-binding protein-like (NUBPL) plays a critical role in complex I assembly. Recessive variants in the *NUBPL* gene are causative for a rare mitochondrial complex I deficiency disorder. Previous studies have investigated the pathogenicity of *NUBPL* mutations in complex I assembly in the yeast model. In particular, a yeast mimic of the patient-specific variant, *NUBPL* p.L102P significantly reduced the NUBPL protein stability and complex I assembly, suggesting that this variant leads to significant loss of NUBPL function, thus disrupting complex I assembly [2].

*Correspondence: vkimonis@uci.edu

[1] Division of Genetics and Genomic Medicine, Department of Pediatrics, University of California, Irvine, CA, USA
Full list of author information is available at the end of the article

Cheng *et al. Orphanet Journal of Rare Diseases*   (2022) 17:386

Page 2 of 12

The NUBPL gene was first reported as a cause of mitochondrial complex I deficiency (MIM 613621, 618242) in 2010 in a whole exome sequencing (WES) study of over 100 patients with clinical and biochemical evidence of complex I deficiency [3]. Six additional patients were identified from a magnetic resonance imaging (MRI) database of more than 3000 subjects with unclassified diffuse leukodystrophy involving the cerebellar cortex, periventricular deep and subcortical white matter and corpus callosum with some cystic changes [4]. All patients from this study had c.815-27T>C in cis with c.166G>A plus a second deleterious NUBPL variant in trans. Three more families were reported to have NUBPL disease [2–8].

We recently reported four new patients with compound heterozygous variants in the *NUBPL* gene, among whom two families had the *NUBPL* p. L104P variant [9]. The affected individuals presented with ataxia, cerebellum hypoplasia, global developmental delay, and one patient had a Leigh-like phenotype variant [9]. Literature review identified one additional family who was compound heterozygous with the p. L104P *NUBPL* variant [9], the other allele being the branch-site c.815-27T>C variant. Studies have suggested that this splicing site variant c. 815-27T>C can lead to incidences of exon 10 skipping and intron inclusion, thus reducing the normal NUBPL mRNA level [2, 9]. Notably, the c. 815-27T>C occurs at a frequency of 1.2% in the European population, which suggests that this variant is mild. The more severe p. L104P variant has not been well-characterized in the population, and its function in a rodent model has yet to be determined.

To understand the role of *NUBPL* variants in disease pathogenesis, we generated the *Nubpl* global knockout mice, and the patient-specific *Nubpl* p. L104P knock-in mice using CRISPR/Cas9 technology. Consistent with the prior studies [10], we found early embryonic lethality in both homozygous models, indicating that the *NUBPL* p. L104P variant is deleterious and behaves similar to the null allele.

A recent report suggests that loss of function in *NUBPL* may increase the susceptibility of Parkinson's disease (PD) in adulthood [11]. Since the aging phenotype of the heterozygote mice had not been studied, we examined the PD-associated behaviors in aging *Nubpl* heterozygous mice to investigate a possible link between NUBPL deficiency and PD.

Methods

Generation of the heterozygous *Nubpl*^L104P+/− knock-in mice using CRISPR/Cas9 technology

Nubpl^104P+/- mice were generated using CRISPR/Cas9. C57BL6N/J pronuclear staged zygotes were injected with gRNAs (2uM each), Cas9 protein (3uM IDT), and p. L104P ssODN repair template. The resulting offspring were genotyped and sequenced. Founder mice with the p. L104P variant were mated with C57BL6N/J. F1 generation p. L104P mice were sequenced to confirm mutant sequence (F primer: 5′ AGCTATCCCAGGCAATTT ATACTT 3′; R primer: 5′ GCCTGGAAAGTGAACAGT AGGT 3′). Subsequent genotyping used Taqman probes (Nubpl WT probe: CTTGTTAGATGTGGATGT; Nubpl mutant probe: CTTGCCAGACGTCGAC). The mice have been backcrossed for 10 generations to remove the contaminating background.

Generation of the hemizygous *Nubpl* knock out mice

Nubpl Knockout first (reporter-tagged insertion with conditional potential) ES cells and mice (allele name: *Nubpl*^tm1a(EUCOMM)WTSI), MGI:4363128) were generated by the International Mouse Knockout Consortium (https://www.mousephenotype.org/), via a mouse embryonic stem (ES) cell-targeting approach using C57BL/6NTac ES cells, such that exon 4, a critical exon, has the KO first cassette inserted.

Embryo harvesting of the homozygous Nubpl knockout and *Nubpl*^L104P/L104P mice

Heterozygous mice were mated and embryos were timed based on detection of a vaginal plug. The following morning was considered to be 0.5 dpc. At 9.5–11.5 dpc pregnant females were sacrificed by cervical dislocation and the uterine horns dissected out. Individual embryos were removed from the placentae and placed in individual wells of a Corning Costar 12-well plate and imaged. Images were taken using a ProgRes Speed XT^core5 Jenoptik camera attached to a Leica M165-C stereomicroscope with a Leica Objective Planapo 0.63x lens and integrated LED ring light. Genotyping was performed at Transnetyx with self-designed primer sets.

Behavioral tests of hemizygous Nubpl knockout mice

The hemizygous *Nubpl* mice were subject to a battery of tests (Table 1) as previously described [6] at 14 months to identify PD-like phenotypes. Behavioral tests were conducted at MRC Mouse Genetics Research Institute. Terminal behavioral analyses were based on The Adult Phenotype Pipeline from the International Mouse Phenotyping Consortium (IMPC) (Table 1) (https://www.mousephenotype.org/impress/index).

mRNA analysis to confirm expression

mRNA was isolated from heterozygous brain and quadricep muscle. cDNA was made from mRNA using random priming. Nubpl was amplified by PCR using forward primer CTACCACCGCAGTGAACCTT and reverse

Table 1 Evaluation of aging *Nubpl*+/− mice

Motor	Aging parameters	Vision	Emotionality
Open field	Tremor	Visual placing	Aggression
Grip strength	Vocalization	Lens mass	Startle response
Contact righting	Fat mass	Overall health of cornea, eye, eyelid, iris, pupil, retina, eye vasculature	
Gait	Bone mineral content and density		
Head bobbing			

primer CAAACAAGTGGCGCAGTCTC. PCR product was column purified and Sanger sequenced.

Animal care and approvals

This study was approved by the University of California Irvine Office of Research Institutional Animal Care & Use Committee (IACUC), Protocol #AUP19-075 and Stanford University School of Medicine IACUC Protocol #31890. Mice were housed on a standard 12 h of light-dark cycle and ad libitum food and water. *Nubpl*$^{L104P+/-}$ and C57BL/6J mice were used for immunohistochemistry and immunofluorescence

Tissue harvest and treatment

Animals were transcardially perfused with 50 ml of PBS (4 °C). Brains were harvested and embedded in optimal cutting temperature media (OCT, Sakura, 4583) for sectioning and sectioned 15 μm-thick tissue sections on a cryostat (Thermo Scientific, Model HM525NX) and placed the sections onto Fisherbrand Superfrost Plus slides (Thermo Scientific, 12-550-15).

Fluorescent immunohistochemistry

Immunostaining was performed in brains from male mice with *Nubpl*$^{L104P+/-}$ and C57BL/6J genotypes. 15 um-thick coronal sections were fixed in 10% neutral buffered formalin (Sigma-Aldrich, MKLK5486), washed with phosphate buffer saline (PBS), then permeabilized and blocked with 0.3% Triton X-100 (Sigma Aldrich, MKBF3357B), 3% bovine serum albumin (BSA) and 5% normal goat serum (NGS) in PBS for 30 minutes at room temperature. Then sections were incubated for 3 hours at room temperature with the following primary antibodies; rabbit anti-alpha-synuclein antibody (Cell Signaling, clone: D37A6, 4179BF) diluted at 1:200 or anti-nubpl antibody (Abcam, clone: EPR11833, ab171741) diluted at 1:500. After incubation with the primary antibody, sections were washed three times with PBS and incubated for 2 hours at room temperature with the following secondary antibodies: Alexa Fluor goat anti-mouse 647 (Invitrogen, A32728) and Alexa Fluor 647 anti-rabbit (Invitrogen, A27040). Nuclear counterstain was performed using a 1:10,000 Hoechst solution in PBS for five minutes. Finally, sections were mounted using ProLong Gold Antifade Mountant reagent (Invitrogen, P36930) and imaged using an ImageExpress Pico epifluorescent microscope (Molecular Devices).

Chromogenic immunohistochemistry

Oxidative stress markers oxoguanine and nitrotyrosine were labeled in striatal and mesencephalic 15 um-thick coronal sections. After fixation in 10% neutral buffered formalin, sections were washed with PBS, endogenous peroxidase activity was blocked with 3% hydrogen peroxide (H_2O_2) for 15 min in PBS followed by two distilled water wash steps and a final PBS wash step. Tissue blocking was performed with 5% BSA in PBS for 30 minutes.

Primary antibodies for goat anti-oxoguanine (8-Ohdg) (dilution of 1:500) or rabbit anti nitrotyrosine antibody (dilution of 1:500) were incubated overnight at 4 °C. VisuCyte horseradish peroxidase (HRP) polymers (R&D systems, VC003 or VC004) were used to tag and were revealed with an Impact 3, 3′-diaminobenzidine (DAB) substrate kit peroxidase (Vectamount, SK-4105). Sections were dehydrated and cleared with ethanol and xylene followed by mounting with permanent mounting media

---

(See figure on next page.)

Fig. 1 Generation of *Nubpl*$^{104P+/-}$ knockout *Nubpl*$^{-/-}$ mice indicated in figure as *Nubpl*$^{-/-}$ and *Nubpl* p. L104P knock-in mice. **A** Schematic showing *Nubpl*^{tm1a} knockout allele. **B** *Nubpl* homozygous knockout mice were sub-viable at E9.5. **C** *Nubpl* p. L104P CRISPR design. Additional silent mutations added to inhibit Cas9 cutting of p. L104P mutation. **D** Sequences of *Nubpl*$^{104P+/-}$ heterozygous mouse for the p. L104P (TT>CC) variant. Multiple silent variants were introduced to reduce recurrent CRISPR/Cas9 targeting. **E** *Nubpl* L104P/L104P homozygous (designated as NUBPL LP/LP) mice were embryonically lethal
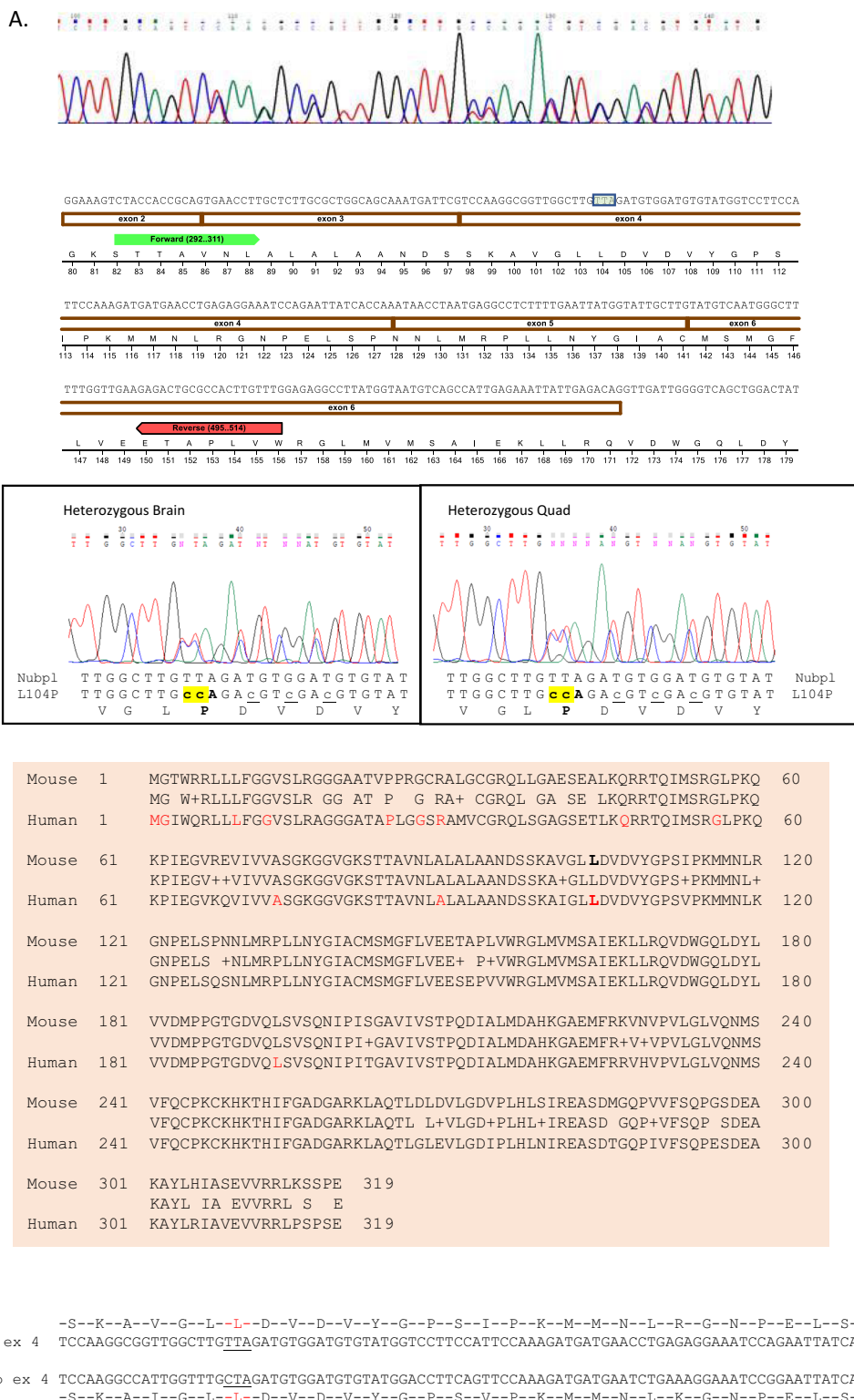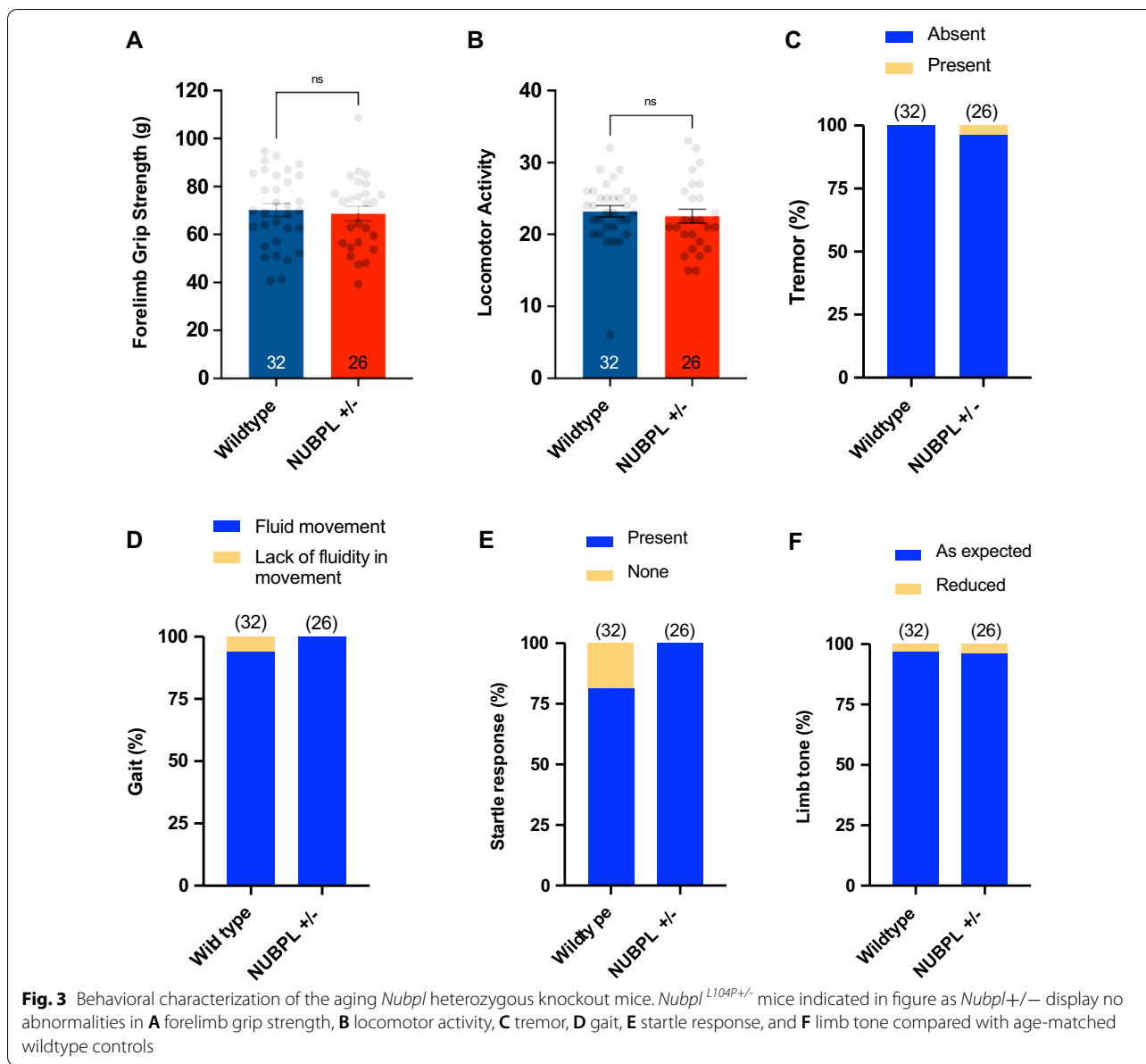
A *Nubpl -/- mouse*

B E9.5

WT   NUBPL +/-   NUBPL -/-

C *Nubpl p.L104P* Knock-in mouse (*Nubpl* LP) CRISPR design

Mouse Nubpl   Exon 4

AATCTTTTGATGATTTTGGTTTTCTTGCAGTCCAAGGCGGTTGGCTTGTTAGATGTGGATGTGTATGGTCCTTCCATTCCAAAGATGATGAACCTGAGAGG
AAATCCAGAATTATCACCAAGTGAGTACAGAAAA

gRNA 1 GGCGGTTGGCTTGTTAGATG TGG   sense (0.5326) g166

AATCTTTTGATGATTTTGGTTTTCTTGCAGTCCAA**GGCGGTTGGCTTGTTAGATG**TGGATGTGTATGGTCCTTCCATTCCAAAGATGATGAACCTGAGAGGAA
ATCCAGAATTATCACCAAGTGAGTACAGAAAA

gRNA2 ATCTAACAAGCCAACCGCCT TGG   anti (0.5047) g167
        coding seq ccaAGGCGGTTGGCTTGTTAGAT

AATCTTTTGATGATTTTGGTTTTCTTGCAGT**CCAAGGCGGTTGGCTTGTTAGAT**GTGGATGTGTATGGTCCTTCCATTCCAAAGATGATGAACCTGAGAGGAA
ATCCAGAATTATCACCAAGTGAGTACAGAAAA

ssODN mutates L104P, at both PAM sites, bases 1-8 in sgRNA and adds Sal1 restriction site
AACCTGATGAATAATCTTTTGATGATTTTGGTTTTCTTGCAGTCtAAaGCcGTTGGCTTGccaGAcGTcGAcGTGTATGGTCCTTCCATTCC
AAAGATGATGAACCTGAGAGGAAATCCA

```
            S   K   A   V   G   L   L   D   V   D   V   Y   G   P   S
GGTTTTCTTGCAGTCCAAGGCGGTTGGCTTGTTAGATGTGGATGTGTATGGTCCTTCC        WT
|||||||||||||||| || || ||||||||| ||| || |||||||||||||||||
GGTTTTCTTGCAGTCtAAaGCcGTTGGCTTGccaGAcGTcGAcGTGTATGGTCCTTCC        ssODN
            S   K   A   V   G   L   P   D   V   D   V   Y   G   P   S
```

D *Nubpl p.L104P* Knock-in mouse (*Nubpl* LP)

```
WT      1 CTTGCAGTCCAAGGCGGTTGGCTTGTTAGATGTGGATGTGTATGGTCCTTCC 52
          ||||||||| |||| |||||||||||| ||||  || || ||||||||||||||
Mutant  1 CTTGCAGTCTAAAGCCGTTGGCTTGCCAGACGTCGACGTGTATGGTCCTTCC 52
                  S   L   A           L>P  D   V   D
```

E E10.5

WT   *Nubpl* LP/LP   *Nubpl* LP/LP

Fig. 1 (See legend on previous page.)

Fig. 2 Expression of Nubpl *p. L104P* allele by cDNA sequencing. **A** Relatively similar levels of wild type and *p. L104P* is expressed. **B** PCR primers span multiple exons and exon splice junctions were correctly confirmed. Silent mutations downstream of *p. L104P* mutation were added to inhibit cutting by Cas9 Crispr during mouse model development. **C**, **D** Nubpl mouse: human amino acid homology. Known disease associated aa mutations are shown in red

Cheng *et al. Orphanet Journal of Rare Diseases* (2022) 17:386

Page 6 of 12

Fig. 3 Behavioral characterization of the aging *Nubpl* heterozygous knockout mice. *Nubpl* [L104P+/-] mice indicated in figure as *Nubpl*+/− display no abnormalities in **A** forelimb grip strength, **B** locomotor activity, **C** tremor, **D** gait, **E** startle response, and **F** limb tone compared with age-matched wildtype controls

(Vectamount, H5008). No hematoxylin and eosin (H&E) counterstain was performed.

Results

Previous studies have suggested that the *Nubpl* global knockout mouse is mid-gestationally lethal, partially due to defects in placenta development. To understand the role of *Nubpl* variants in disease pathogenesis and mouse development, we generated a knock-in mouse containing patient-specific variant *Nubpl p. L104P* using CRISPR/Cas9 technology (Figs. 1, 2). The NUBPL L104 amino acid residue is conserved between human and mouse. Sanger sequencing results indicated successful knock-in of *Nubpl p.L104P* allele (Fig. 2). To confirm the
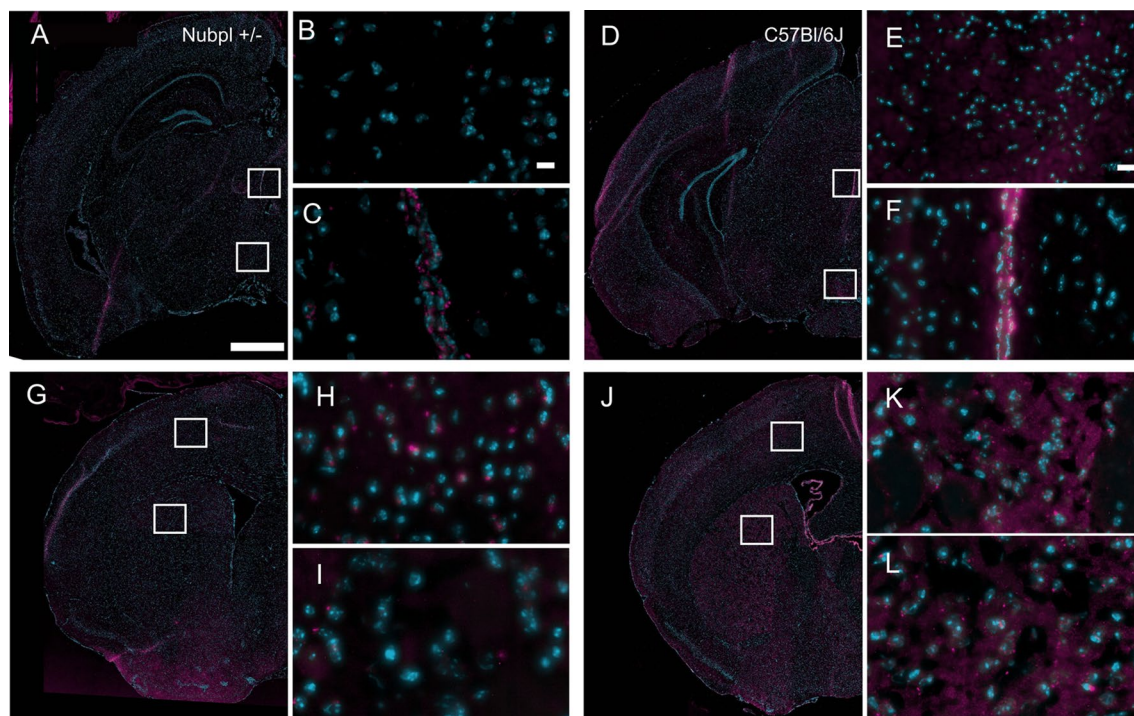
Fig. 4 Nubpl immunofluorescence in *Nubpl* $^{L104P+/-}$ mice indicated in figure as Nubpl+/− and C57BL/6J brains. **A**, **D**, **G**, **J** Panoramic hemi-brain; Nubpl expression in magenta and nuclear counterstain (Hoechst) in blue. Approximate coordinate -3 anteroposterior (AP) related to Bregma; **A**–**C** Mesencephalic coronal section of a *Nubpl*$^{L104P+/-}$ male; **G**–**I** Striatal section of Nubpl +/- male; D-F. Mesencephalic coronal section; **J**–**L** Striatal coronal section of a 10 months old C57BL/6J control male; **C**, **F** magnification of the third ventricle; **B**, **E** Zoom into the interpeduncular nucleus of the mesencephalon; **H K** Magnification in the caudoputamen; **I**, **L** Magnification in the cortex. Scale bar for **A**, **G** represents 500 μm; **B**, **E**, represents 10 μm

expression of mutant allele, we harvested total mRNA from mouse brain cortex and performed reverse transcription to synthesize cDNA. We performed PCR to obtain the amplicon that contains the *p. L104P* mutation, followed by Sanger sequencing. Both wildtype and mutant mRNA are expressed. Furthermore, we obtained the *Nubpl* global knockout mouse from The European Mutant Mouse Archive (EMMA) (Fig. 1). Consistent with the prior study [4], we found early embryonic lethality in both models. In particular, *Nubpl* knockout mice were sub-viable at E9.5; only 3 knockout embryos were obtained out of 43 embryos. *Nubpl* $^{L104P/-}$ was born with expected Mendelian ratio. No embryos were obtained for *Nubpl* $^{L104P/L104P}$ at E10.5 (Fig. 1D, E). These data indicate that the *NUBPL p. L104P* variant behaves similar to a null allele.

Additionally, previous studies have shown that embryonic placental defects correlate strongly with abnormal brain development [10]. In particular, genetic knockout mice with placenta defects tend to display abnormal forebrain morphology later on [10]. Interestingly, patients with *NUBPL*-associated mitochondria complex I deficiency disorders also manifest severe neurodevelopmental abnormalities including cognitive deficit and cerebellar atrophy. Recently, a patient case report revealed that haploinsufficiency resulting from having one allele of *NUBPL* may increase the susceptibility of developing Parkinson's disease (PD) in adulthood [11]. Therefore, we examined PD-associated behaviors in aging *Nubpl* hemizygous mice to further investigate the link between NUBPL deficiency and PD. At 14-month old, the *Nubpl* hemizygous mice were subject to a battery of aging
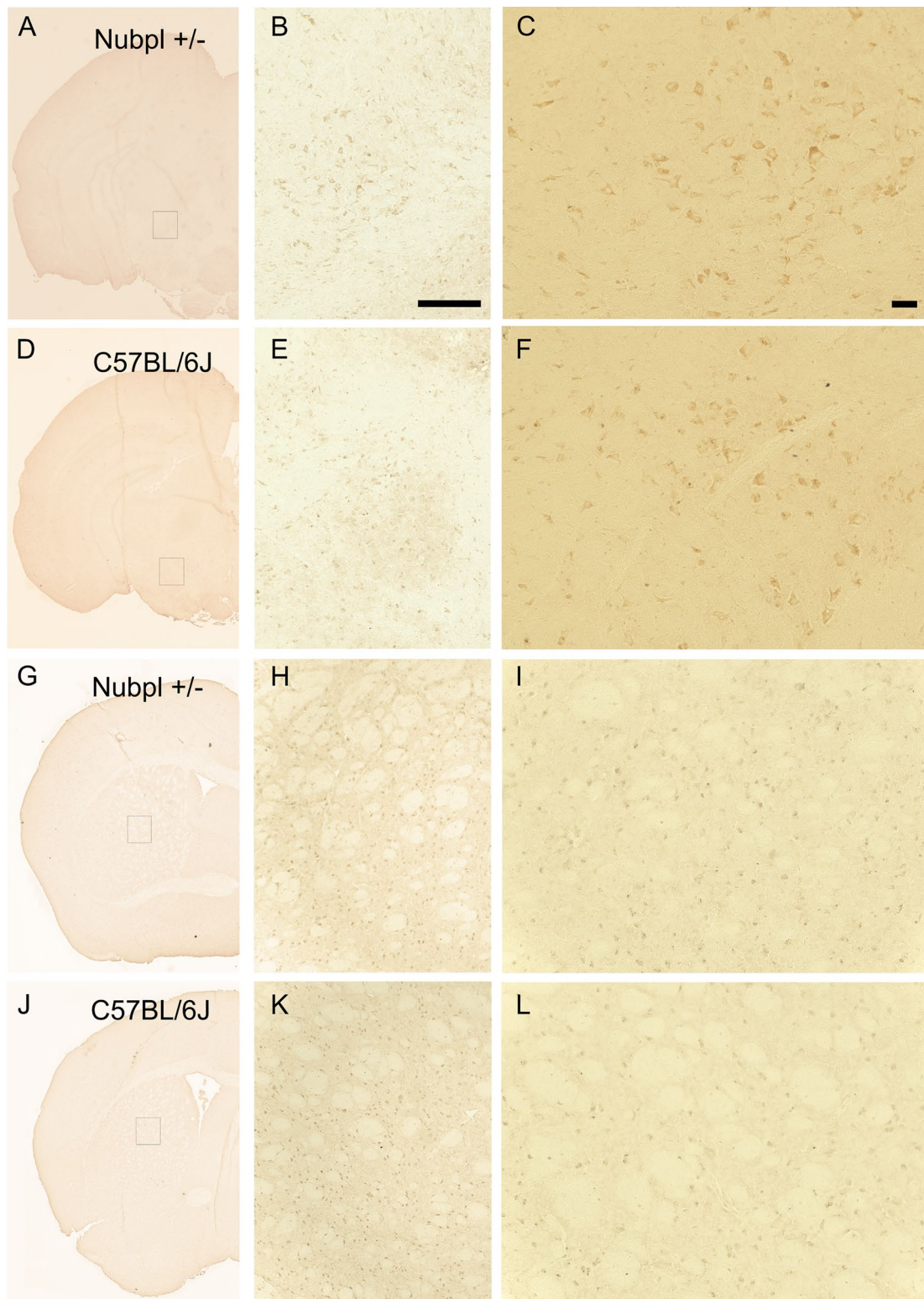
Fig. 5 NTT (nitrotyrosine) expression in *Nubpl$^{L104P/-}$* mice indicated in figure as Nubpl +/− and C57BL/6J brains. **A**–**C**, **G**–**I** Panoramic 3,3′-Diaminobenzidine (DAB) hemi-brain staining of Nubpl+/− male; **D**–**F**, **J**–**L** Hemi-brain stain of a 10-month old C57BL/6J control male; **B**, **E** Zoom in the third ventricle; **C**, **F** Magnification of the third ventricle; **H**, **K** Zoom in the caudoputamen-lateral ventricle; **I**, **L** Magnification of the caudoputamen-lateral ventricle. Scale bar for **B** represents 250 μm, for C represents 100 μm

Cheng *et al. Orphanet Journal of Rare Diseases*   (2022) 17:386

Page 9 of 12
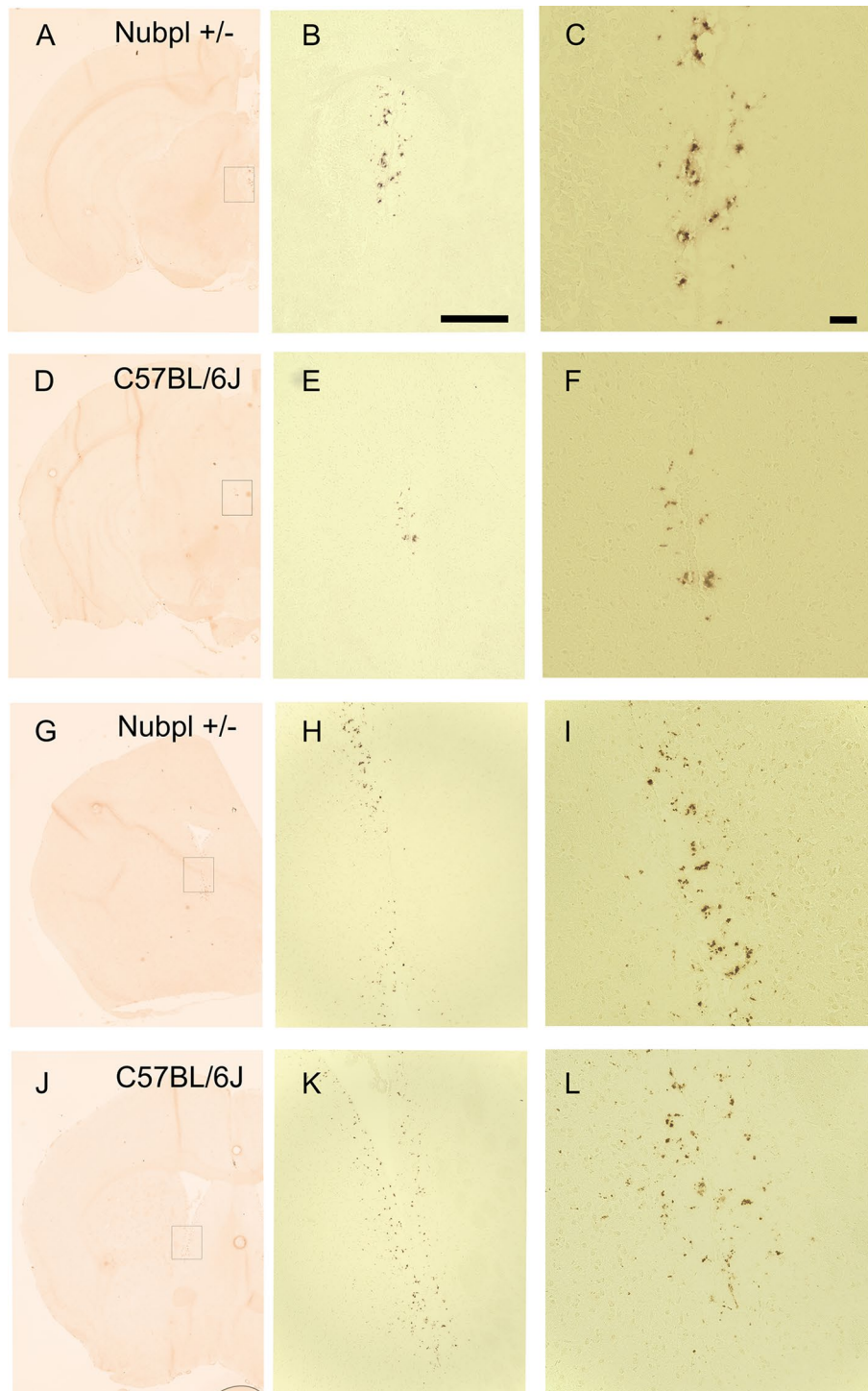
Fig. 6 8-Oxoguanine (8-OHDG) expression in *Nubpl L104P/-* mice indicated in figure as Nubpl +/− and C57BL/6J brains. **A**–**C**, **G**–**I** Panoramic 3,3′-Diaminobenzidine (DAB) hemi-brain staining of Nubpl+/− male; **D**–**F**, **J**–**L** Hemi-brain stain of a 10-month old C57BL/6J control male; **B**, **E** Zoom in the substantia nigra (SN); **C**, **F** Magnification of the SN; **H**, **K** Zoom in the caudoputamen. **I**, **L** Magnification of the caudoputamen. Scale bar **B** scale bar: 250 μm, **C** 100 μm

Cheng *et al. Orphanet Journal of Rare Diseases*   (2022) 17:386

Page 10 of 12

phenotype screens with a high-throughput phenotyping pipeline with automated phenotype-detection strategy and visualization [12]. These tests cover a wide spectrum of behavioral and phenotypic analyses, including motor behaviors, aging parameters, vision, and emotionality tests (Fig. 3; Table 1). The *Nubpl* hemizygous mice revealed no significant abnormalities compared to the age and gender-matched wild-type mice. In particular, *Nubpl* hemizygous mice did not display reduced functional performance and feet clasping.

To characterize the pathological changes in *Nubpl* hemizygous mice, Nubpl protein was analyzed by immunofluorescence. In the *Nubpl* hemizygous mice, we found an overall decreased expression of Nubpl in both the striatal and mesencephalic sections compared to the C57BL/6J strain (Fig. 4). Histological analysis of the PD-related protein alpha-synuclein was performed to characterize the expression pattern in the two main brain regions affected in PD: striatum and substantia nigra. This analysis did not show any changes in alpha-synuclein expression compared to a 10-month-old C57BL/6J mouse (Fig. 7), which supports the behavioral and phenotypic analysis.

NUBPL is a Fe/S protein that plays a critical role in the assembly of the respiratory complex I, part of the respiratory chain in the mitochondria [13, 14]. Depletion or impairment of the correct assembly of the respiratory chain could cause an increase in reactive oxygen species leading to an increase in oxidative stress [15, 16]. Therefore, we also evaluated nitrotyrosine (NTT) and oxoguanine (8-Ohdg) with immunohistochemistry. There were no evident changes in the expression patterns of these two oxidative stress markers (Figs. 5, 6).

Discussion

Our studies have provided insights into the pathogenicity of the *NUBPL* p. L104P variant. Patients harboring the *NUBPL* p. L104P variant display severe cerebellar degeneration along with intellectual disability and global developmental delay [3]. Previous studies characterizing the yeast mimics of NUBPL p. L104P mutation suggest that this amino acid change likely results in misfolding of the NUBPL protein. We found that the *Nubpl* p. L104P

mouse was lethal at the mid-gestational stage, similar to the *Nubpl*-null mouse, thus it is likely that the p. L104P variant is a hypomorph that mimics the null allele. Thus, a tissue-specific knockout model of *Nubpl* might be a more advantageous model to help delineate the function of NUBPL and pursue therapeutic strategies for complex I deficiency disorders.

Despite our intention to determine the complex I activity in the NUBPL p. L104P homozygous mice, it is difficult because embryonic lethality happens too early in the developmental stage to obtain enough tissue to perform both genotyping experiments and complex I activity assay for each embryo. For the same reason, we could not perform histological analysis for the mutant embryos. Moreover, establishing cell lines including mouse embryonic fibroblast is challenging with normally developed embryos from E9-E10, let alone defective embryos due to NUBPL deficiency.

Even though we did not observe significant behavioral abnormalities in aging *Nubpl* heterozygous mice, we cannot exclude the possibility that partial loss of function leads to increased susceptibility to PD. It is plausible that our end-point behavioral analysis was not sensitive enough to detect abnormalities or PD-associated behaviors, or mice were not sufficiently aged to detect one. At 14 months, we also did not detect frank neuropathology related to oxidative stress or accumulation of alpha-synuclein. Older mice may manifest late-onset PD-like features. In future analysis, a brain-specific knockout model may also provide more insights into how NUBPL plays a role in the central nervous system.

Altogether, our attempt to generate a mouse model of *NUBPL*-associated mitochondrial deficiency has suggested that strategies of global knock-in with *Nubpl p. L104P* and *Nubpl* knockout are deleterious to embryogenesis, and future studies will be critical to understanding and bypass the role of NUBPL in early development. Generation of tissue-specific *Nubpl* knockout or knock-in mice that harbor less deleterious variants to understand disease pathogenesis is necessary to help in developing models to study potential treatments for this rare severe disorder.

(See figure on next page.)
Fig. 7 Alpha-synuclein expression in *Nubpl^(L104P/-)* mice indicated in figure as Nubpl+/− and C57BL/6J brains. **A**, **F**, **K**, **P** Panoramic hemi-brain; alpha-synuclein in magenta and nuclear counterstain (Hoechst) in blue. Approximate AP coordinate -3 related to Bregma; A-E. Mesencephalic coronal section of a Nubpl+/− male, **K**–**O** Striatal section of Nubpl+/− male; **F**–**J** Mesencephalic coronal section; **P**–**T** Striatal coronal section of a 10-month-old C57BL/6J control male; **B**, **G** Zoom into the hippocampal formation including the dental gyrus granule cell layer, polymorph layer, and molecular layer; **C**, **H** Magnification of the dentate gyrus, polymorph layer; **D**, **I** Zoom into the substantia nigra, reticular part, and part of the cerebal peduncle; **E**, **J** Magnification of the substantia nigra, reticular part; **L**, **Q** Zoom in the caudoputamen; **M**, **R** Magnification in the caudoputamen; **N**, **S** Zoom into the cortex; **O**, **T** Magnification in the cortex. Scale bar for **A**, **F** represents 500 µm, **B**, **D**, **G**, **I** represents 100 µm, **C**, **E**, **H**, **J** represents 10 µm
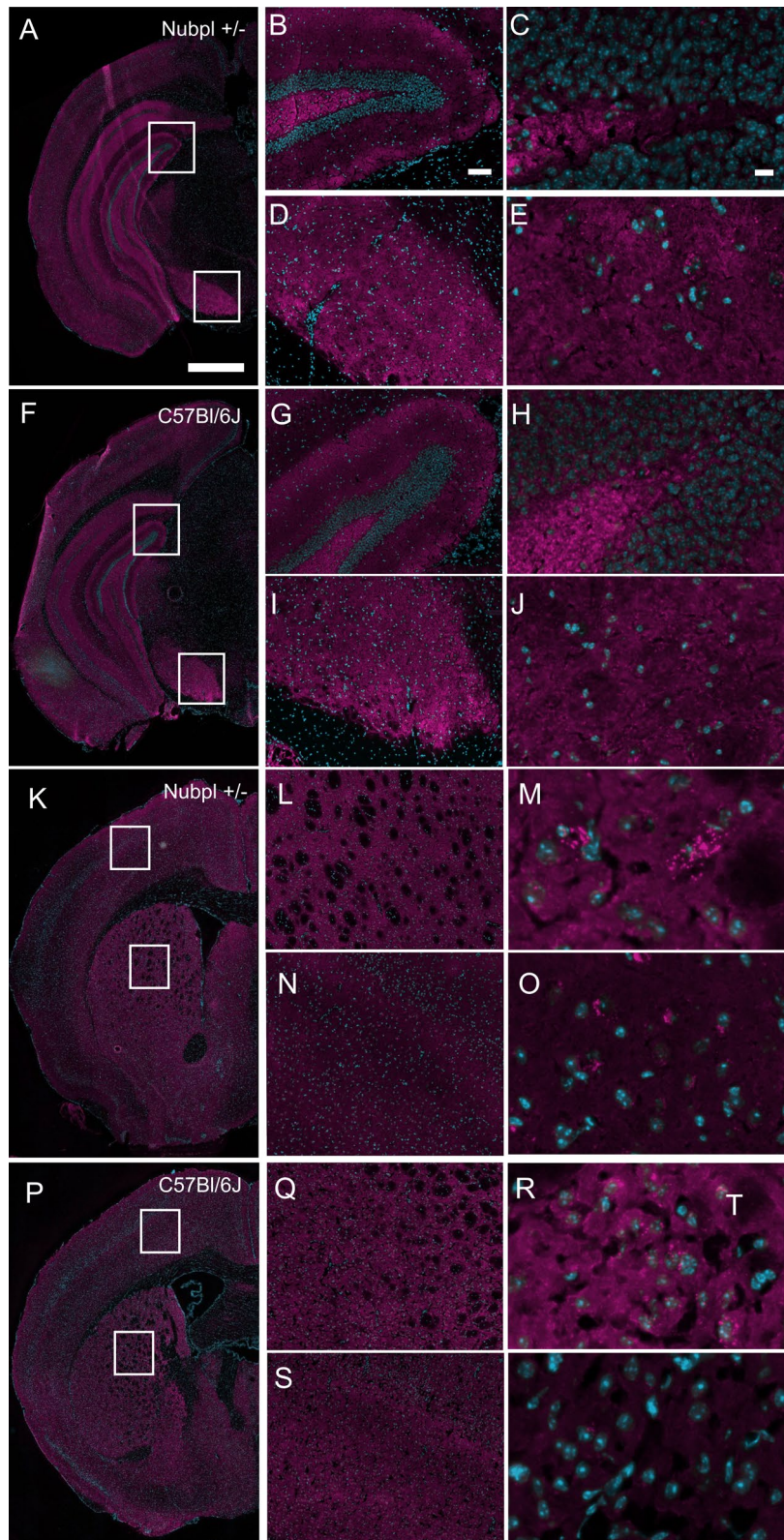
Cheng *et al. Orphanet Journal of Rare Diseases*   (2022) 17:386

Page 11 of 12

Fig. 7 (See legend on previous page.)

Cheng *et al. Orphanet Journal of Rare Diseases*   (2022) 17:386

Page 12 of 12

Declarations

Ethics approval and consent to participate

Animal experiments were approved by the University of California Irvine Office of Research Institutional Animal Care & Use Committee (IACUC), Protocol #AUP19-075 and Stanford University School of Medicine IACUC, Protocol #.31890. The study protocol conformed to the ethical guidelines of the 1975 Declaration of Helsinki and was approved by the Ethics Committee of UC Irvine.

Consent for publication

Not applicable. This study did not utilize any human material.

Competing interests

The authors declare no competing interests.

Author details

[1]Division of Genetics and Genomic Medicine, Department of Pediatrics, University of California, Irvine, CA, USA. [2]Mary Lyon Centre, MRC Harwell Institute, Harwell Campus, Oxfordshire OX11 0RD, UK. [3]Department of Pathology, Stanford University School of Medicine, Stanford, CA, USA. [4]Transgenic Mouse Facility, University of California, Irvine, CA, USA. [5]Population Bio UK, Inc, Begbroke Science Park, Begbroke, UK. [6]Department of Neurology, University of California, Irvine, CA, USA. [7]Department of Pathology, University of California, Irvine, CA, USA. [8]Department of Environmental Medicine, University of California, Irvine, CA, USA. [9]Children's Hospital of Orange County, Orange, CA, USA.

References

1. Wirth C, Brandt U, Hunte C, Zickermann V. Structure and function of mitochondrial complex I. Biochim Biophys Acta. 2016;1857(7):902–14.
2. Maclean AE, Kimonis VE, Balk J. Pathogenic mutations in NUBPL affect complex I activity and cold tolerance in the yeast model Yarrowia lipolytica. Hum Mol Genet. 2018;27(21):3697–709.
3. Calvo SE, Tucker EJ, Compton AG, Kirby DM, Crawford G, Burtt NP, et al. High-throughput, pooled sequencing identifies mutations in NUBPL and FOXRED1 in human complex I deficiency. Nat Genet. 2010;42(10):851–8.
4. Kevelam SH, Rodenburg RJ, Wolf NI, Ferreira P, Lunsing RJ, Nijtmans LG, et al. NUBPL mutations in patients with complex I deficiency and a distinct MRI pattern. Neurology. 2013;80(17):1577–83.
5. Balint B, Charlesworth G, Stamelou M, Carr L, Mencacci NE, Wood NW, et al. Mitochondrial complex I NUBPL mutations cause combined

dystonia with bilateral striatal necrosis and cerebellar atrophy. Eur J Neurol. 2019;26(9):1240–3.
6. Protasoni M, Bruno C, Donati MA, Mohamoud K, Severino M, Allegri A, et al. Novel compound heterozygous pathogenic variants in nucleotide-binding protein like protein (NUBPL) cause leukoencephalopathy with multi-systemic involvement. Mol Genet Metab. 2020;129(1):26–34.
7. Tenisch EV, Lebre AS, Grevent D, de Lonlay P, Rio M, Zilbovicius M, et al. Massive and exclusive pontocerebellar damage in mitochondrial disease and NUBPL mutations. Neurology. 2012;79(4):391.
8. Friederich MW, Perez FA, Knight KM, Van Hove RA, Yang SP, Saneto RP, et al. Pathogenic variants in NUBPL result in failure to assemble the matrix arm of complex I and cause a complex leukoencephalopathy with thalamic involvement. Mol Genet Metab. 2020;129(3):236–42.
9. Kimonis V, Al Dubaisi R, Maclean AE, Hall K, Weiss L, Stover AE, et al. NUBPL mitochondrial disease: new patients and review of the genetic and clinical spectrum. J Med Genet. 2021;58(5):314–25.
10. Perez-Garcia V, Fineberg E, Wilson R, Murray A, Mazzeo CI, Tudor C, et al. Placentation defects are highly prevalent in embryonic lethal mouse mutants. Nature. 2018;555(7697):463–8.
11. Eis PS, Huang N, Langston JW, Hatchwell E, Schule B. Loss-of-function NUBPL mutation may link parkinson's disease to recessive complex I deficiency. Front Neurol. 2020;11:555961.
12. Potter PK, Bowl MR, Jeyarajan P, Wisby L, Blease A, Goldsworthy ME, et al. Novel gene function revealed by mouse mutagenesis screens for models of age-related disease. Nat Commun. 2016;7:12444.
13. Wydro MM, Balk J. Insights into the pathogenic character of a common NUBPL branch-site mutation associated with mitochondrial disease and complex I deficiency using a yeast model. Dis Model Mech. 2013;6(5):1279–84.
14. Mimaki M, Wang X, McKenzie M, Thorburn DR, Ryan MT. Understanding mitochondrial complex I assembly in health and disease. Biochim Biophys Acta. 2012;1817(6):851–62.
15. Cui H, Kong Y, Zhang H. Oxidative stress, mitochondrial dysfunction, and aging. J Signal Transduct. 2012;2012:646354.
16. Guo C, Sun L, Chen X, Zhang D. Oxidative stress, mitochondrial damage and neurodegenerative diseases. Neural Regen Res. 2013;8(21):2003–14.

Publisher's Note

Springer Nature remains neutral with regard to jurisdictional claims in published maps and institutional affiliations.